

# Binary mixture of hard disks as a model glass former: Caging and uncaging

Sin-iti Sirono<sup>1, a)</sup>

*Earth and Environmental Sciences, Nagoya University, Tikusa, Nagoya 464-8601, Japan*

(Dated: 17 August 2021)

I have proposed a measure for the cage effect in glass forming systems. A binary mixture of hard disks is numerically studied as a model glass former. A network is constructed on the basis of the colliding pairs of disks. A rigidity matrix is formed from the isostatic (rigid) sub-network, corresponding to a cage. The determinant of the matrix changes its sign when an uncaging event occurs. Time evolution of the number of the uncaging events is determined numerically. I have found that there is a gap in the uncaging timescales between the cages involving different numbers of disks. Caging of one disk by two neighboring disks sustains for a longer time as compared with other cages involving more than one disk. This gap causes two-step relaxation of this system.

PACS numbers: 61.43.Fs, 64.70.pv, 64.70.pm

## I. INTRODUCTION

When a glass-forming material is cooled, the motion of the constituents becomes extremely slow. Likewise, the mobility of a granular material decreases as the grains are tightly packed. Although the glass forming materials are thermal and the granular material is athermal, many features similar to that of glass-forming materials have been found in a granular system<sup>1</sup>. This similarity suggests a common mechanism in these systems. The motion of the constituents is restricted due to their neighbors. This is called 'cage effect'<sup>2</sup>. Clearly, the cage effect is of geometrical origin, regardless of whether a material is thermal or athermal. If a constituent cannot escape from a cage after cooling or packing has taken place, the system freezes. This is observed as glass transition or jamming transition for granular materials. The cage effect plays a critical role in these transitions.

The cage effect has been studied using various procedures. A plateau in the time evolution of the mean square displacement has been found<sup>2,3</sup> between the initial ballistic regime and the later diffusive regime. A constituent rattles inside a cage during the plateau. The intermediate scattering function displays a two-step relaxation in accordance with the mean square displacement<sup>2,3</sup>. Cage correlation function<sup>4</sup> defined by the list of neighbor's successively reproduces the temperature dependence of a diffusion constant. Three point velocity correlation function captures the correlation of directions of motion between different times, and shows a backward motion of constituents caused by a cage<sup>5</sup>. Non-Gaussian parameter reveals that the velocity distribution of the constituents deviates upwardly at a high velocity range from a simple Gaussian distribution, corresponding to a correlated motion induced by a cage<sup>6</sup>. The four point correlation

function<sup>7</sup> shows the correlations between the relaxation of different constituents. The jump of a constituent<sup>8</sup> can be divided into two types: reversible and irreversible. The ratio of irreversible to reversible jumps increases with temperature, corresponding to an increase in the escape from a cage.

All of these functions or measures deal with the motion of the caged constituents. The effects of a cage are discussed indirectly through the motion of the caged constituents. There is no measure directly dealing with the caging constituents adjoining to the caged constituents. I have proposed a measure for the cage effect based on the determinant of the rigidity matrix<sup>9</sup>. The concept of rigidity has been applied to network glasses<sup>10</sup>, and fluid-solid transition<sup>11</sup>.

I have selected a mixture of hard disks, which has already been investigated by many authors<sup>12-14</sup>, as a model glass former. The disks collide with each other elastically, without energy dissipation. As the packing fraction  $\phi$  (fractional area occupied by disks) increases, a two-step relaxation of the density fluctuation<sup>5</sup> is observed in this system.

In the next section, I define a local network of interacting disks, characterizing a cage. I introduce a parameter which quantifies the caging in Section 3. Numerical methods are explained in Section 4. Numerical results are presented in Section 5. Section 6 gives discussions and conclusions.

## II. LOCALLY RIGID FRAMEWORK

Figure 1 shows two examples of the cage effect. The red disk caged between two black disks [Fig. 1(a)] cannot pass through between the two disks to the other side unless the gap between the two disks increases up to the diameter of the red disk. Likewise, a triangle of three disks constrained by the three surrounding disks [Fig. 1(b)] cannot

<sup>a)</sup>sirono@eps.nagoya-u.ac.jp

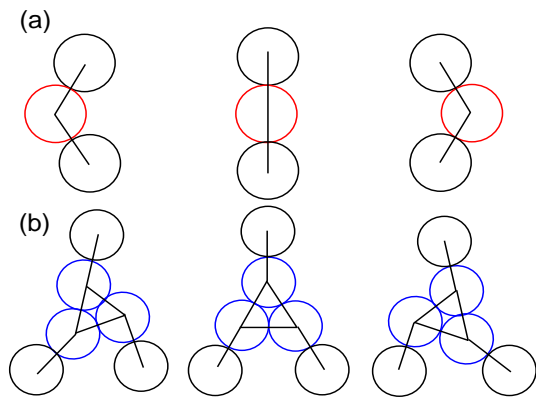


FIG. 1. (color online). Schematics of the cage effect. (a) Red disk is caged between two black disks. The red disk cannot pass through between the two disks (from the left to the right) unless the gap between the black disks is larger than the diameter of the red disk (middle). Fictitious networks representing contacts between disks are shown by black lines. (b) A cluster of three blue disks is caged by three black disks.

rotate unless the top disk shifts upwards such that the two triangles, one of which is formed by the centers of the three caged disks, and the other consists of the centers of the surrounding disks, are perspective from a line (the extensions of three pairs of corresponding sides of the two triangles meet in collinear points<sup>15</sup>).

If we apply an external force to the red disk to make it pass through between the two caging disks or to the blue disks to rotate the triangle, force carrying networks are formed as shown by the black bonds in Fig. 1 provided that the positions of the end disks are fixed. If we place hinges at the centers of the disks connected by rigid bonds rotating freely around the hinges, the networks in Fig. 1 are rigid and isostatic<sup>16</sup>, such that any removal of a bond results in a network that is not rigid. If the number of the caged disk is  $N_{\text{disk}}$ , the number of columns of the matrix

is  $2N_{\text{disk}}$  (there are two bonds in Fig. 1(a) ( $N_{\text{disk}} = 1$ ) and six bonds in Fig. 1(b) ( $N_{\text{disk}} = 3$ )). This is a property of an isostatic network.

In the disk system, the combination of the colliding pair of the caged disks does not change for a short timescale. From the list of colliding pairs, we can construct a network where each bond represents the colliding disk pair. If a disk (or a set of disks) is caged, we can find a set of bonds corresponding to those shown in Fig. 1. This is because the condition of uncaging shown in Fig. 1 is the same even if the disks move and collide with each other. Therefore, we can define an isostatic sub-network in the network as a cage. This local sub-network of bonds is called the 'locally rigid framework (LRF)'. An LRF inhibits the motion of a disk (or a set of disks) in one particular direction. If all LRFs pertaining to a disk are effective, the disk can only rattle inside the cage. It should be noted that this network is not a real contact network, but a fictitious one because the disks do not continue to contact but they collide. Moreover, an LRF may be broken as the system evolves and distances between the disks increase.

### III. CAGING PARAMETER

An uncaging event can be detected by the rigidity matrix<sup>9</sup>. We can construct the rigidity matrix from the LRF such that each row represents a bond and each column corresponds to the coordinates of caged disks. An LRF consists of bonds inside caged disks in addition to bonds connecting between a caged disk and a neighboring caging disk. There are two bonds connecting a caged disk (red) and caging disks (black) in Fig. 1(a). For Fig. 1(b), there are three bonds inside the caged disks (blue) and three bonds connecting the caged disks and caging disks (black).

If there are bonds between the caged disks 1 – 2 and 2 – 3, the rigidity matrix is written as<sup>9</sup>

$$\begin{array}{c} \text{bonds} \\ \begin{array}{l} 1 - 2 \\ 2 - 3 \\ \dots \end{array} \end{array} \left( \begin{array}{cccccc} \text{coordinates of the caged disks} & & & & & & \\ \begin{array}{l} x_1 \quad y_1 \quad x_2 \quad y_2 \quad x_3 \quad y_3 \quad \dots \\ \frac{x_1-x_2}{d_{12}} \quad \frac{y_1-y_2}{d_{12}} \quad \frac{x_2-x_1}{d_{21}} \quad \frac{y_2-y_1}{d_{21}} \quad 0 \quad 0 \quad \dots \\ 0 \quad 0 \quad \frac{x_2-x_3}{d_{23}} \quad \frac{y_2-y_3}{d_{23}} \quad \frac{x_3-x_2}{d_{32}} \quad \frac{y_3-y_2}{d_{32}} \quad \dots \\ \dots \end{array} \end{array} \right), \quad (1)$$

where  $x_i$  and  $y_i$  are the positions of the  $i$ -th disk, and  $d_{ij} = \sqrt{(x_i - x_j)^2 + (y_i - y_j)^2}$  is the distance between the centers of disks  $i$  and  $j$ . It should be noted that the matrix is not symmetrical with exchanging  $i$  and  $j$ . If  $i$ -th disk is caged by  $j$ -th caging disk, the matrix contains  $(x_i - x_j)/d_{ij}$  but does not contain  $(x_j - x_i)/d_{ij}$ .

The rigidity matrix for an isostatic network is a square matrix (the number of degrees of freedom of the caged

disks  $2N_{\text{disk}}$  and the number of bonds are the same in an isostatic network<sup>9</sup>) and has a determinant except for a special position of the disks<sup>9</sup> when uncaging occurs.

When the red disk passes between the other two disks in Fig. 1(a), the determinant of the LRF becomes zero because the two bonds are in parallel when the three centers of the disks are collinear. The determinant changes its sign at this point. Likewise, the sign of the determi-

nant in the right panel is different from that in the left panel in Fig. 1(b).

Using the determinant of the LRF with  $N_{\text{disk}}$  caged disks, we can define the caging parameter  $\chi_{N_{\text{disk}}}$ , which is a measure of the effectiveness of cages. It is defined as

$$\chi_{N_{\text{disk}}}(t) = 1 - \frac{\Pi_{N_{\text{disk}}}(t)}{\Sigma_{N_{\text{disk}}}}, \quad (2)$$

where,  $\Sigma_{N_{\text{disk}}}$  is the number of LRFs investigated which have  $N_{\text{disk}}$  caged disks, and  $\Pi_{N_{\text{disk}}}(t)$  is the number of LRFs whose determinants change their sign among  $\Sigma_{N_{\text{disk}}}$ . It should be noted that the number  $\Pi_{N_{\text{disk}}}(t)$  is increased by one when a determinant changes its sign, only if an LRF has not been broken such that the lengths of all the bonds  $d_{ij}$  are less than  $f(R_i + R_j)$ , where  $R_i$  is the radius of the  $i$ th disk. The factor  $f = 1.5$  is adopted here.

#### IV. NUMERICAL METHODS

To determine the evolution of  $\chi_{N_{\text{disk}}}(t)$ , the positions of disks should be known. The evolution of the positions of hard disks can be efficiently computed by an event-driven simulation<sup>14</sup>, in which the collision times between disks and velocities after collisions are sequentially solved. Disks having two different radii, 1.0 and 1.4 in dimensionless units, are mixed in equal proportions. This size ratio has been chosen to safely avoid crystallization<sup>13</sup>. The total number of disks is 1024. A periodic boundary condition is applied. The packing fraction of the disks  $\phi$  is 0.8. The initial velocity distribution is Gaussian with unit variance in dimensionless units. I have defined the colliding pair of the disks in a particular time window of 200 in the normalized unit. The fictitious network is constructed from the list of colliding disks in the time window.

In order to construct an LRF, a circular region is first placed randomly on the fictitious network. The disks and the connecting bonds inside the circle are chosen. By varying the radius of the circle, the number of disks inside the circle is changed between three and hundred, which is much smaller than the system size (1024 disks). The number of chosen bonds is usually more than that required for an isostatic network. This is because the disks move and have a chance to collide with more disks than when they are tightly packed.

Overconstraining bonds (their removal does not affect the rigidity of the network) are randomly removed until the isostatic condition<sup>17</sup> is fulfilled. An example of an isostatic network is shown in Fig. 2. If a bond is further removed from the isostatic network, some fraction of the bonds becomes mobile. Correspondingly, a disk (or a set of disks) also becomes mobile (rotates around a disk center). For example, if we remove a blue bond at the bottom of Fig. 2, another blue bond becomes mobile and the disk connected by this blue bond can rotate around. We can find a minimum set of mobile bonds among  $2N_{\text{disk}}$

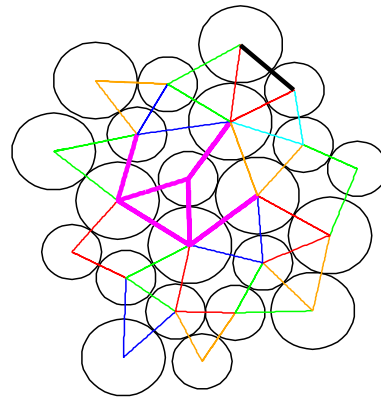


FIG. 2. (color online). An example of LRFs. Disks and bonds are chosen in a circular region in the computational area. Sets of bonds denoted by different colors are identified as LRFs on the basis of the rigidity of the local sets of bonds. An LRF of 6 bonds is denoted by the thick pink lines. The thick black line is the residual bond after decomposition

possible bond removals. The mobile bonds can be found by the pebble game algorithm<sup>17</sup>.

In addition to the removed bond, the induced mobile bonds are further removed from the isostatic network. In the example above, we remove two blue bonds from the network. An LRF is composed of this local mobile network plus the removed bond. The remaining network, after the removal, is still isostatic. During each removal of bonds, the mobile disk (caged disk) is also removed accordingly. The disks adjacent to the mobile disk connected through the removed bonds correspond to the caging disks. This removal process is repeated. Finally, the isostatic network is uniquely decomposed into the sets of LRFs plus one bond (thick black bond in Fig. 2). In Fig. 2, there are 17 LRFs with 2 bonds ( $N_{\text{disk}} = 1$ ) and 1 LRF with 6 bonds ( $N_{\text{disk}} = 3$ ) shown by pink lines. The pattern of LRFs shown in Fig. 2 changes if the position of the randomly chosen circular region is shifted or the random sequence of the removal of the overconstraining bonds is changed.

According to this procedure, the LRF of  $N_{\text{disk}} = 2$  is impossible because we can always find an immobile bond for a particular removal of a bond. An LRF of  $N_{\text{disk}} = 2$  splits into two LRFs of  $N_{\text{disk}} = 1$ .

#### V. NUMERICAL RESULTS

##### A. Two-step relaxation

Black curves in Fig. 3 display the evolution of  $\chi_{N_{\text{disk}}}$ . From the right to the left of the black curves, the number of caged disk  $N_{\text{disk}}$  is 1, 3, 5, and 10. As  $N_{\text{disk}}$  increases,  $\chi_{N_{\text{disk}}}$  decreases faster. All  $\chi$ s start to decrease at  $t = 10^{-2}$ , when the intermediate scattering function  $F_{q_{\text{max}}}(t)$  starts the first relaxation.  $F_{q_{\text{max}}}(t)$  is given by  $\langle \sum_i \exp(\mathbf{q}_{\text{max}}(\mathbf{x}_i(t) - \mathbf{x}_i(0))) \rangle$ , where  $\mathbf{x}_i$  is the position

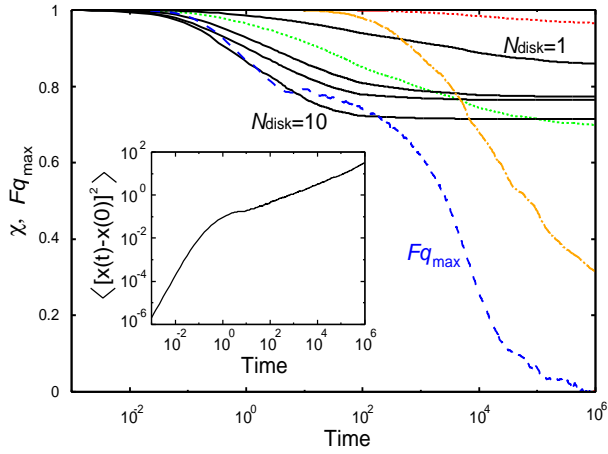


FIG. 3. (color online). Decrease in caging parameter  $\chi_{N_{\text{disk}}}(t)$  for various  $N_{\text{disk}}$  at  $\phi = 0.8$ . From right to left, the black (solid) curves correspond to  $N_{\text{disk}} = 1, 3, 5,$  and  $10$ . The red (upper dotted) curve represents the subset of  $N_{\text{disk}} = 1$  in which a bond exists between the two caging disks when the bonds are placed according to the colliding pairs. The green (lower dotted) curve corresponds to the other group in which no bond is placed between the caging disks. The orange (dotted-dashed) curve is the same as the red (upper dotted) curve but  $\Pi_{N_{\text{disk}}}(t)$  in Eq. (2) is multiplied by a factor of 20. The blue (dashed) curve is the intermediate scattering function (self-part)  $F_{q_{\text{max}}}(t)$  at the wave number  $q_{\text{max}}$  where structure factor is maximum. [inset: mean square displacement]

of the  $i$ -th disk, the angular bracket is the ensemble average, and  $q_{\text{max}}$  is the wave number at which the structure factor is the maximum. This function measures the relaxation of the structure with the nearest-neighbor length scale. This first period corresponds to the ballistic motion of the disks before a collision as can be seen in the inset of Fig. 3 where the mean square displacement, defined by  $\langle [x_i(t) - x_i(0)]^2 \rangle$ , increases as  $t^2$ . The LRFs uncaged during this stage are essentially ineffective, or very weak.

$F_{q_{\text{max}}}(t)$  reaches a plateau when  $t \simeq 4$ . All  $\chi$ s continue to decrease after  $F_{q_{\text{max}}}(t)$  reaches the plateau. We cannot find any coincidence between  $\chi$ s (solid curves) and the second relaxation of  $F_{q_{\text{max}}}(t)$ .

The decrease in  $\chi_3, \chi_5,$  and  $\chi_{10}$  ceases when  $t \simeq 10^2$ . All LRFs belonging to these  $\chi$ s are uncaged or broken by this time.

The decrease in  $\chi_1$  (the rightmost black curve) is clearly distinct from the others. There is a gap in the uncaging times between  $\chi_1$  and  $\chi_3$ . The uncaging time (the time when  $\chi_{N_{\text{disk}}}(t) = 0.9$ ) for  $\chi_1$  is larger than that for  $\chi_3$  by a factor of  $1.8 \times 10^3$  (Fig.4(a)). It should be noted that there is no particular behavior in  $\chi_1$  at  $t \simeq 10^2$ , when  $F_{q_{\text{max}}}(t)$  starts its second relaxation.

This gap is emphasized if we divide the LRFs of  $N_{\text{disk}} = 1$  into two groups. In one group  $\chi_{1,\text{LO}}$ , there is a bond between the two caging disks, when the bond

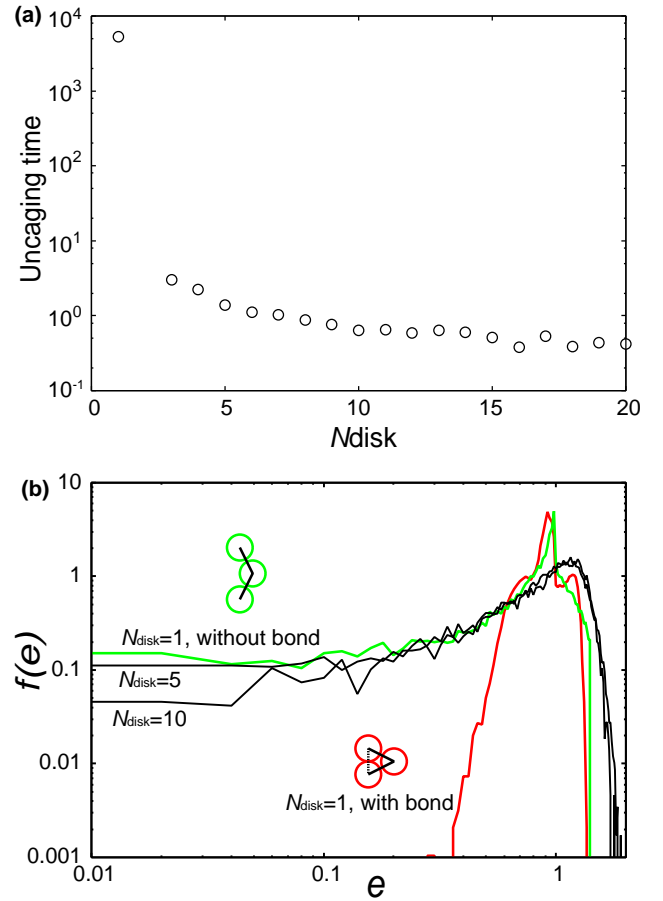


FIG. 4. (color online). Gaps between cages. (a) Uncaging time as a function of  $N_{\text{disk}}$ . (b) The distribution of the absolute value of the eigenvalue  $e$  of the rigidity matrix. The red curve stands for  $N_{\text{disk}} = 1$  with a bond between the two caging disks, and the green curve for  $N_{\text{disk}} = 1$  without the bond. The two black curves are for  $N_{\text{disk}} = 5$  and  $N_{\text{disk}} = 10$ .

is placed on the basis of the colliding pairs. In the other group  $\chi_{1,\text{WK}}$ , no bond is placed between the caging disks (schematics are shown in Fig. 4(b)). The decrease in  $\chi_{1,\text{LO}}$  and  $\chi_{1,\text{WK}}$  are shown as the red (upper dotted) and green (lower dotted) curves respectively, in Fig. 3. The green curve starts to decrease at the same period to other  $\chi$ s and continues to decrease through  $t \simeq 10^2$  without any notable change.

On the other hand,  $\chi_{1,\text{LO}}$  starts to decrease at  $t \simeq 10^2$ . Interestingly, this period coincides with the onset of the second relaxation of  $F_{q_{\text{max}}}(t)$ . There is no special signature at  $t = 10^2$  in other  $\chi$ s. The amount of the decrease in  $\chi_{1,\text{LO}}$  is small, because more than 90% of the LRFs investigated are broken before uncaging. The orange (dotted-dashed) curve is the same as the red curve, but  $\Pi_{N_{\text{disk}}}(t)$  in Eq. (2) is multiplied by a factor of 20 to make a comparison with  $F_{q_{\text{max}}}(t)$ . A good coincidence can be seen between the second relaxation of  $F_{q_{\text{max}}}(t)$  and  $\chi_{1,\text{LO}}$ .

## B. Gap between cages

Figure 4(a) shows the uncaging time (the time when  $\chi_{N_{\text{disk}}}(t) = 0.9$ ) as a function of  $N_{\text{disk}}$ . It can be seen that the uncaging time of LRFs with  $N_{\text{disk}} = 1$  is significantly larger than those of other  $\chi$ s. The uncaging time of other  $\chi$ s decreases with  $N_{\text{disk}}$ . A determinant  $M$  of an LRF can be factorized such that  $M = HS$ , where  $H$  is composed of the bonds of an isostatic subgraph (a triangle) in an LRF, and  $S$  depends on the pattern of the rest of the LRF<sup>15</sup>. A determinant of an LRF can be decomposed into factors corresponding to triangles and to connecting bonds between triangles. A factor for a triangle cannot change its sign because the LRF is broken before the change. Therefore, the change in sign of a determinant for  $N_{\text{disk}} \geq 3$  comes from the factors of connecting bonds between triangles. Because the number of such factors contained in  $M$  increases as  $N_{\text{disk}}$ , the uncaging time decreases as  $N_{\text{disk}}$ .

The distribution  $f(e)$  of the absolute value  $e$  of a complex eigenvalue of the rigidity matrix when  $t = 0$  is shown in Fig. 4(b).  $f(e)$  is defined such that  $f(e)de$  is the fraction of the eigenvalues between  $e$  and  $e + de$  and that  $\int f de = 1$ . The eigenvalues evolve with time followed by the evolution of the disk position. When one of the eigenvalues of a rigidity matrix goes to zero, the determinant changes its sign. Thus, the eigenvalue  $e$  measures the difficulty of the uncaging. As  $e$  increases, the displacements of the disks required for uncaging increases. An eigenvalue corresponds to an eigenfrequency if there is a harmonic potential between the disks. It can be seen that there is a substantial fraction of low frequency modes for  $N_{\text{disk}} \geq 3$  in addition to  $N_{\text{disk}} = 1$  without a bond. On the other hand, the distribution  $f(e)$  for  $N_{\text{disk}} = 1$  with a bond falls to zero at  $e = 0.3$ . This difference is the origin of the gap in uncaging times. An LRF with small  $e$  uncages faster. However, an LRF consisting of tightly packed disks sustains for a long time.

## VI. DISCUSSION AND CONCLUSION

These observations suggest that the uncaging of LRFs of  $N_{\text{disk}} = 1$  with a bond ( $\chi_{1,\text{LO}}$ ) requires the uncaging of other LRFs. Uncaging of LRFs with  $N_{\text{disk}} \geq 3$  and  $N_{\text{disk}} = 1$  without a bond proceeds during the plateau of the intermediate scattering function. The LRFs relaxed in the first stage flip over again between the neighboring configurations as shown in the left and right panels in Fig. 1. The system gradually changes its configuration by the flipping of the weak LRFs relaxed in the first stage. The plateau shows that the disk system requires time to find a configuration to open a path between two disks packed initially with an order.

Displacements of disks due to the uncaging of these LRFs are small, and can be seen as a plateau of the mean square displacement when  $t \simeq 10$ , as shown in the inset of Fig. 3. This period corresponds to  $\beta$  relax-

ation of glass forming materials<sup>3</sup>. Disk positions gradually change in this period and the distance between two caging disks in LRFs with  $N_{\text{disk}} = 1$  with a bond, enlarges. The uncaging of LRFs with  $N_{\text{disk}} = 1$  with a bond triggers a large structural change and promotes the second relaxation of  $F_{q_{\text{max}}}(t)$ . This period corresponds to  $\alpha$  relaxation of glass forming materials<sup>3</sup>. The requirement of uncaging of other types of LRFs for LRFs with  $N_{\text{disk}} = 1$  with a bond is the situation of “constrained dynamics”<sup>18</sup> which explains the slow relaxation of glass-forming systems. According to this study, uncaging of LRFs  $N_{\text{disk}} = 1$  with a bond cannot take place by itself. Through the uncaging of LRFs with  $N_{\text{disk}} \geq 3$  and  $N_{\text{disk}} = 1$  without a bond, the arrangement of the disks changes so that uncaging of LRFs  $N_{\text{disk}} = 1$  with a bond takes place.

An LRF with  $N_{\text{disk}} = 1$  with a bond is the collection of locally ordered packing of three disks because the three disks collide with each other when the network is determined. This local order cannot propagate throughout because of the poly-dispersity of the disks. This situation is called the geometrical frustration<sup>19</sup>. Because of the lack of the long-range order, the geometrical frustration inevitably leads to the formation of weak LRFs, which are uncaged first.

In conclusion, I have proposed a measure for the cage effect of a binary mixture of disks. I have found the gap between cages with different numbers of caged disks. Cages with one disk relax slower than those involving more than one disk. The former cages correspond to the locally ordered packing of disks. The latter cages represent disordered packing of disks. This coexistence of locally ordered and disordered disks leads to the two step relaxation.

## ACKNOWLEDGMENTS

- <sup>1</sup>P. M. Reis, R. A. Ingale, and M. D. Shattuck, Phys. Rev. Lett. **98**, 188301 (2007).
- <sup>2</sup>E. Donth, *The glass transition: relaxation dynamics in liquids and disordered materials* (Springer, 2001).
- <sup>3</sup>K. Binder and W. Kob, *Glassy materials and disordered solids: An introduction to their statistical mechanics* (World scientific, 2005).
- <sup>4</sup>E. Rabani, J. D. Gezelter, and B. J. Berne, J. Chem. Phys. **107**, 6867 (1997).
- <sup>5</sup>B. Doliwa and A. Heuer, Phys. Rev. Lett. **80**, 4915 (1998).
- <sup>6</sup>E. R. Weeks and D. A. Weitz, Phys. Rev. Lett. **89**, 095704 (2002).
- <sup>7</sup>E. Flenner and G. Szamel, J. Phys. Cond. Mat. **19**, 205125 (2007).
- <sup>8</sup>K. Vollmayr-Lee, J. Chem. Phys. **121**, 4781 (2004).
- <sup>9</sup>J. Graver, *Counting on frameworks* (The Mathematical Association of America, 2001).
- <sup>10</sup>J. C. Phillips, “Rigidity theory and applications,” (Kluwer, New York, 1999) pp. 155–171.
- <sup>11</sup>A. Huerta and G. G. Naumis, Phys. Rev. Lett. **90**, 145701 (2003).
- <sup>12</sup>B. J. Alder and T. E. Wainwright, Phys. Rev. **127**, 359 (1962).
- <sup>13</sup>R. J. Speedy, J. Chem. Phys. **110**, 4559 (1999).
- <sup>14</sup>M. Isobe, Int. J. Mod. Phys. C **10**, 1281 (1999).
- <sup>15</sup>N. L. White and W. Whiteley, SIAM J. Alg. Disc. Meth. **4**, 481 (1983).

<sup>16</sup>C. Moukarzel and P. M. Duxbury, Phys. Rev. Lett. **75**, 4055 (1995).

<sup>17</sup>D. J. Jacobs and M. F. Thorpe, Phys. Rev. Lett. **75**, 4051 (1995).

<sup>18</sup>R. G. Palmer, D. L. Stein, E. Abrahams, and P. W. Anderson, Phys. Rev. Lett. **53**, 958.

<sup>19</sup>J.-P. Sadoc and R. Mosseri, *Geometrical frustration* (Cambridge University Press, 1999).